Full length article

Development of osteopromotive poly (octamethylene citrate glycerophosphate) for enhanced bone regeneration ☆

Yun He [a,1], Qiyao Li [b,*,1], Chuying Ma [b], Denghui Xie [c], Limei Li [a], Yitao Zhao [c], Dingying Shan [b], Sarah K. Chomos [b], Cheng Dong [b], John W. Tierney [b,d], Lin Sun [e], Di Lu [a], Li Gui [f,*], Jian Yang [b,*]

[a] Biomedicine Engineering Research Centre, Kunming Medical University, Kunming 650500, Yunnan, China
[b] Department of Biomedical Engineering, Materials Research Institute, The Huck Institutes of the Life Sciences, The Pennsylvania State University, University Park, PA, USA
[c] Academy of Orthopedics, Guangdong Province, Guangdong Provincial Key Laboratory of Bone and Joint Degenerative Diseases, The Third Affiliated Hospital of Southern Medical University, Guangzhou 510280, Guangdong, China
[d] Department of Biomedical Engineering, College of Engineering and Computing, University of South Carolina, Columbia, SC, 29201, USA
[e] Department of Cardiology, The Second Affiliated Hospital, Kunming Medical University, Kunming 650101, Yunnan, China
[f] Department of Endocrinology, The Third People's Hospital of Yunnan Province, Kunming 650011, Yunnan, China

ARTICLE INFO

ABSTRACT

The design and development of bioactive materials that are inherently conducive for osteointegration and bone regeneration with tunable mechanical properties and degradation remains a challenge. Herein, we report the development of a new class of citrate-based materials with glycerophosphate salts, β-glycerophosphate disodium (β-GP-Na) and glycerophosphate calcium (GP-Ca), incorporated through a simple and convenient one-pot condensation reaction, which might address the above challenge in the search of suitable orthopedic biomaterials. Tensile strength of the resultant poly (octamethylene citrate glycerophosphate), POC-βGP-Na and POC-GP-Ca, was as high as 28.2 ± 2.44 MPa and 22.76 ± 1.06 MPa, respectively. The initial modulus ranged from 5.28 ± 0.56 MPa to 256.44 ± 22.88 MPa. The mechanical properties and degradation rate of POC-GP could be controlled by varying the type of salts, and the feeding ratio of salts introduced. Particularly, POC-GP-Ca demonstrated better cytocompatibility and the corresponding composite POC-GP-Ca/hydroxyapatite (HA) also elicited improved osteogenic differentiation of human mesenchymal stem cells (hMSCs) *in vitro*, as compared to POC-βGP-Na/HA and POC/HA. The superior *in-vivo* performance of POC-GP-Ca/HA microparticle scaffolds in promoting bone regeneration over POC-βGP-Na/HA and POC/HA was further confirmed in a rabbit femoral condyle defect model. Taken together, the tunability of mechanical properties and degradation rates, together with the osteopromotive nature of POC-GP polymers make these materials, especially POC-GP-Ca well suited for bone tissue engineering applications.

Statement of Significance

The design and development of bioactive materials that are inherently conducive for osteointegration and bone regeneration with tunable mechanical properties and degradation remains a challenge. Herein, we report the development of a new class of citrate-based materials with glycerophosphate salts, β-glycerophosphate disodium (β-GPNa) and glycerophosphate calcium (GPCa), incorporated through a simple and convenient one-pot condensation reaction. The resultant POC-GP polymers showed significantly improved mechanical property and tunable degradation rate. Within the formulation investigated, POC-GPCa/HA composite further demonstrated better bioactivity in favoring osteogenic differentiation of hMSCs *in vitro* and promoted bone regeneration in rabbit femoral condyle defects. The development of POC-GP expands the repertoire of the well-recognized citrate-based biomaterials to meet the ever-increasing needs for functional biomaterials in tissue engineering and other biomedical applications.

1. Introduction

Over 2.2 million bone grafting procedures are performed annually worldwide [1] in orthopedics, neurosurgery and dentistry, rendering bone substitutes increasingly necessary and applied clinically. The development of fully synthetic bone substitutes that are readily available, cost-effective, and osteo-promotive is particularly encouraged in the clinical field [2]. Despite significant progress, currently available synthetic materials are limited by their inabilities to mimic native tissue composition, weak mechanical strength, significant inflammatory responses, poor bone integration, and slow bone regeneration [3]. Inspired by natural bone, a native biocomposite comprised of collagen as the major organic component providing the naturally derived polymeric framework for inorganic calcium phosphate (CaP) mineral nucleation, inorganic bioceramics, such as hydroxyapatite (HA), and tricalcium phosphate (TCP), have been introduced into biodegradable synthetic polymers to create biomimetic composites aimed at better resembling the native bone composition [4–7].

Citrate, highly accumulated in natural bone, has been found to strongly bind to bone inorganic minerals, playing indispensable roles in stabilizing the mineral crystals [8] and controlling crystal size [9]. As a robust multifunctional monomer, citrate chemistry enables the formation of a 3D cross-linked network structure when reacted with different diols [10,11] as well as providing rich pendant carboxyl and hydroxyl groups to allow the incorporation of up to 65 % weight of HA, closely resembling the inorganic composition of natural bone. During the past decade, a series of citrate-based material/HA composites have been developed in our lab and have demonstrated impressive *in vivo* performance in various animal models for bone regeneration, such as poly(octamethylene citrate)/HA (POC/HA) for osteochondral defect healing [12], clickable POC/HA (POC-click/HA) for long segmental radial bone regeneration [13] and for cranial defect repair [14], citrate-based polymer blends/HA (CBPB/HA) for the repair of lateral femoral condyle defect [15], injectable citrate-based mussel-inspired tissue bioadhesives/HA composites (iCMBA/HA) for comminuted radial bone regeneration [16], as well as N-methyldiethanolamine (MDEA) modified click-crosslinked POC-click/HA (POC-M-click/HA) for spinal fusion [17]. Excitingly, one of our recent studies [18] demonstrated released citrate could promote the differentiation of human mesenchymal stem cells (hMSCs) towards active bone forming cells by regulating energy-producing metabolic pathways. The newly discovered citrate metabonegenic regulation mechanism not only highlights the significance of citrate-based composites for orthopedic applications, but also provides valuable guidance to design materials with improved osteo-promotive functionality. For example, phosphoserine, the native organic phosphate donor in bone, when incorporated in citrate polymer or in its solute form, demonstrates concerted action with citrate leading to accelerated bone formation and maturation [18]. The above studies suggest polymers incorporating phosphates can synergize with citrate to further promote osteogenic differentiation of hMSCs, pointing toward the specific chemical formulation of citrate materials to influence *in vivo* bioactivity.

Mechanical properties are also an important factor of materials that greatly affect tissue engineering efficacy, especially for bone repair [19]. Numerous efforts have been made in our lab to improve the mechanical properties of citrate-based materials, especially for orthopedic applications. Introduction of urethane groups into citrate-based polyester materials has proven to be an effective way for improving mechanical strength but sacrifices the valuable pendant groups for further biofunctionalization and HA chelation [14,20]. Biodegradable elastomers employing click chemistry as an additional crosslinking mechanism have also demonstrated improved mechanical properties; however, these materials display a delayed degradation rate compared with POC, making them unsuitable for applications requiring fast-degrading scaffolds [17,21]. The relatively complex click-monomer synthesis also makes the click-polymers less attractive. Therefore, balancing the mechanical properties and biodegradation rate while introducing biofunctionality into polymer networks in a more convenient way remains as a challenge.

β-glycerophosphate disodium (βGP-Na), widely known as an osteogenic medium supplement and a weak base, has been used to initiate the gelation of chitosan or collagen to generate thermosensitive injectable hydrogels [22]. Another GP salt, glycerophosphate calcium (GP-Ca), representing as a mixture of β-isomer (80 %) and rac-α-isomer (20 %), has long been used as a food supplement for both calcium and phosphate. Given the osteo-promotive benefits of both salts in their solute and conjugated form [23–25], we incorporated two types of GP salts into the citrate-based materials through a one-pot polycondensation reaction by taking advantage of the reactive nature of citric acid, to prepare POC-GP, in order to further improve the bioactivity of citrate materials to promote stem cell osteogenic differentiation. At the same time, our results show that GP incorporation greatly increased the mechanical properties of the resultant polymer. By changing the salt type and feeding ratio and polymerizing the monomers in a very convenient, one-pot polycondensation, the degradation rate of the resulting polymers can also be easily tuned, providing an alternative way to balance mechanical properties, degradation, and bioactivity. A rabbit femoral condyle defect model was used to evaluate the efficacy of POC-GP/HA for bone regeneration. It was observed that the osteopromotive capabilities of GP-doped POC were significantly improved compared with POC and autograft control groups.

2. Materials and methods

2.1. Materials

HA [(particle size: >75 μm (0.5 %), 45–75 μm (1.4 %), <45 μm (98.1 %)] was purchased from Fluka (St Louis, MO). 1,8-octanediol (98 %) and citric acid (99.5 %) were purchased from Alfa Aesar. β-glycerophosphate-Na (βGPNa), Glycerophosphate-Ca (GPCa), and all remaining chemicals were purchased from Sigma-Aldrich (St Louis, MO) and used as received unless stated otherwise.

2.2. Synthesis of pre-polymers

POC pre-polymer was synthesized by bulk polymerization using citric acid and 1,8-octanediol in 1.0:1.1 feeding ratio. Briefly, monomers were stirred mechanically and melted under nitrogen protection at 160 °C in a silicon oil bath. Then the temperature of the system was lowered to 140 °C, followed by stirring for 1–2 h to create the pre-polymer. The reaction was quenched by 1,4-dioxane and purified in deionized water followed by lyophilization. The purified pre-polymer was dissolved in 1,4-dioxane (30 wt/wt%) for further use. POC-βGP-Na and POC-GP-Ca pre-polymers were synthesized via the above method with citric acid, 1,8-octanediol, β-glycerophosphate disodium (β-GP-Na), and glycerophosphate calcium (GP-Ca) in different feeding ratios as shown in Table 1, except that dialysis was performed to purify the pre-polymer before freeze drying.

2.3. Preparation of polymer films, polymer/HA composites and polymer/HA microparticle scaffolds

To prepare polymer films, pre-polymer solutions were cast in Teflon dishes and the solvent was allowed to evaporate. The dried

	Citric acid (M)	1,8-Octandiol (M)	βGP-Na or GP-Ca (M)
POC	1.0	1.1	/
POC-0.2βGP-Na	1.0	0.9	0.2
POC-0.3βGP-Na	1.0	0.8	0.3
POC-0.5βGP-Na	1.0	0.6	0.5
POC-0.2GP-Ca	1.0	0.9	0.2
POC-0.3GP-Ca	1.0	0.8	0.3

pre-polymer was then thermally crosslinked at 80 °C for 3 days and then at 120 °C with vacuum for 1 day to obtain a crosslinked polymer film. To prepare polymer/HA composites, a 30 % pre-polymer solution in 1,4-dioxane was mixed with hydroxyapatite (HA) by continuously stirring. After the mixture turned dough-like, it was then pressed into thin sheets. The composite sheets were cut into round disks then thermally crosslinked at 80 °C for 3 days and at 120 °C with vacuum for 1 day. To prepare the polymer/HA microparticles, porous composite scaffolds were first prepared by mixing pre-polymer solution, HA and NaCl (250–425 μm salt size) followed by casting in Teflon dishes. After the solvent evaporated, the scaffolds were thermally crosslinked as described above and then soaked in de-ionized (DI) water to leach the salt. Next, the porous sponge-like scaffolds were freeze-dried, ground and sieved into different particle sizes (<150 μm; 150–250 μm; 250–425 μm; >425 μm).

2.4. Material characterizations

2.4.1. Structural characterization
To check the chemical structural difference between POC, POC-βGP-Na and POC-GP-Ca, Fourier transform infrared (FT-IR) analysis was operated by casting polymer solution in 1,4-dioxane on KBr pellets using Bruker Vertex V70 spectrometer. FT-IR spectra were recorded over a wavelength range of 400–4000 cm^{-1}. ^{31}P NMR (161.9 MHz) spectra of pre-polymer solutions were obtained using Bruker DPX 400 NMR Spectroscopy. Either D$_2$O or DMSO were used as solvents. All chemical shifts were reported in ppm (δ).

2.4.2. Contact angle measurements
The water-in-air contact angles on crosslinked polymer films were measured at room temperature within 10 s after water was dropped on the film surface by a Rame-Hart goniometer and imaging system (Rame-Hart Inc., Mouttain Lake, NJ) using the sessile drop method. Four independent measurements at different sites were averaged. The change of water-in-air contact angle with time was monitored over 60 s after water dropping.

2.4.3. Tensile mechanical tests
Tensile tests of polymer films were conducted on an Instron 5966 machine equipped with a 1000 N load cell. Samples were cut into rectangular strips and pulled until failure at a speed of 500 mm min^{-1} to obtain stress–strain curves. The initial slope (0–10 %) of the stress–strain curve was used to determine the initial modulus of each sample. Six specimens were averaged for each sample, and the results were presented as mean ± standard deviation.

2.4.4. In vitro degradation and release studies
Degradation properties were studied *in vitro* with polymer film samples placed in tubes containing 10 mL of NaOH solution (0.05 M) or phosphate buffered saline (PBS, pH = 7.4) and incubated at 37 °C. Samples were weighed before degradation to find the initial mass (W$_0$). At each time point, samples were washed thoroughly with deionized water 3 times followed by lyophilization. After

lyophilization, samples were weighed to measure the remaining mass (W$_t$). Six parallel specimens were averaged for each sample, and the results were presented as means ± standard deviation. The percent mass loss was calculated based on the following equation:

$$\text{Mass Loss}(\%) = ((W_0 - W_t)/W_0) \times 100. \quad (1)$$

2.4.5. Phosphorus release studies
Cumulative phosphorus release was investigated by inductively coupled plasma optical emission spectroscopy (ICP-OES 730-ES, Varian, USA) to confirm the presence of βGP-Na and GP-Ca in the release media. Films weighing about 50 mg were soaked in 10 mL of PBS (pH 7.4) solution and incubated at 37 °C. After 14, 21, and 28 days, the release media of each sample were mixed with 10 wt% HNO$_3$ solution at 1:1 ratio and then subjected to ICP-OES measurements.

2.4.6. Morphology of microparticle scaffolds and hMSCs
To observe morphology of microparticle scaffolds and differentiating hMSCs, scanning electron microscopy (SEM, Zeiss Sigma) was used to capture and analyze images at 10 kV. All samples were coated with 5 nm iridium using a Leica sputter coater before imaging.

2.5. Cell culture

In vitro cell studies were performed with human mesenchymal stem cells (hMSCs) in passage 5–7. Growth media (GM) was composed of Dulbecco's Modified Essential Medium (DMEM) supplemented with 10 % fetal bovine serum and 100 units/mL of penicillin-streptomycin. Osteogenic media (OG) was composed of growth media supplemented with 0.5 mM ascorbate-2-phosphate, 100 nM dexamethasone, and 10 mM β-glycerophosphate disodium. Solid samples were submerged in 70 % ethanol for 1 h and sterilized by UV irradiation for 1 h on each surface. For liquid samples, solutions were sterilized by filtering through a sterile syringe filter (0.2 μm cellulose acetate, VWR, PA). For all cell studies, cells were kept in a humidified incubator at 37 °C with 5 % CO$_2$. Both GM and OM were replaced every other day.

2.6. In vitro cytocompatibility evaluation

hMSCs were seeded at 5000 cells/cm^2 and 3000 cells/cm^2 for cell cytotoxicity and cell proliferation, respectively. At each time point, media was removed and hMSCs were rinsed once with PBS solution. 200 μL of cell counting kit-8 (CCK-8) solution was added to each well and incubated at 37 °C for 30 min. The absorbance was measured at a wavelength of 450 nm with a Tecan microplate reader.

2.7. hMSCs differentiation study

To evaluate the hMSCs differentiation on polymer/HA composite disks and microparticle scaffolds, samples were sterilized and transferred to 48-well plates. hMSCs were seeded onto samples at a density of 3000 cells/cm^2 in growth media. Once cells reached 80 % confluency, growth media was removed and replaced with the established osteogenic media or growth media as a general control. To evaluate the effect of GP salt concentrations on osteogenic differentiation, hMSCs were also seeded onto a 48-well plate at a concentration of 10,000 cells/mL in growth medium. Once cells reached 80 % confluency, the growth media was replaced with a reductive osteogenic media (DMEM with 0.5 mM ascorbate-2-phosphate, 100 nM dexamethasone but without

β-glycerophosphate disodium) supplemented with 0.2 mM of different GP salts.

After differentiation for 7, 14, and 21 days, cells were washed 3 times with PBS solution and lysed with 250 μL RIPA buffer for alkaline phosphatase (ALP) assay and DNA quantification. The ALP activity was measured according to the method published previously [18]. The DNA content was tested by Pico Green dsDNA test kit according to manufacturer's instruction. To observe the mineral and ECM formation and cell morphology on polymer/HA composites under SEM, cells were harvested and fixed in 2.5 % glutaraldehyde for 48 h followed by a serial dehydration process, critical-point drying, and iridium sputter coating (Leica Sputtercoater). Gene expression of *Runx-2* (runt-related transcription factor 2), *Col1a1* (encoding collagen type 1 alpha 1), and *SPP1* (encoding osteopontin) were evaluated by real-time PCR. Total RNA was extracted from harvested cells on day 14 with QIAGEN RNeasy kit (Hilden, Germany) and transcribed into cDNA with High-Capacity cDNA Reverse Transcription Kits (Applied Biosystems™, CA). Then real-time PCR was carried out using a QuantStudio Real-Time PCR system (Applied Biosystems™, CA). The primers and TaqMan probe used for human *Runx-2*, *Col1a1*, and *SPP1* were Hs00231692_m1, Hs00164004_m1, and Hs00959010_m1.

2.8. Surgical procedures for animal study

An established femoral condyle defect model on New Zealand white rabbits was used for *in vivo* evaluation according to the method described elsewhere [26,27]. Briefly, a defect with 5 mm in diameter and 5 mm in depth was created at the lateral femoral condyle of each rabbit under continuous saline buffer irrigation, then powders were packed into the defect and the musculature and skin incision were closed with nylon suture. Both the left and right condyles of femur were used. Rabbits were randomly assigned into four groups with different bone implants in left and right legs respectively: 1) sham group (untreated); 2) POC/HA microparticle scaffold group; 3) POC-βGP-Na/HA microparticle scaffold group, and 4) POC-GP-Ca/HA microparticle scaffold group. The concentrations of HA in the composites are all 65 wt%. The particle scaffold with a mixture of different sizes were used for animal studies. After 4, 8, and 12 weeks, 4 rabbits/group were euthanized and subjected to micro-CT analyses. Then the medial femoral condyle and the surrounding tissues were removed, fixed in 4 % phosphate buffered paraformaldehyde solution, sectioned, and stained for histological analysis [28]. A total of 48 New Zealand white rabbits weighing approximately 2.5 kg were used and approved by Kunming Medical University in compliance with all regulatory guidelines. The anesthesia (Pentobarbital Sodium, 30 mg/kg) for all animals was administered through marginal ear veins on the lateral aspect.

2.9. Micro-CT analysis

In order to quantify new bone formation within defects, quantitative imaging of harvested femurs was performed using a micro-CT imaging system (μ-CT80 scanner; Scanco Medical AG, Brüttisellen, Switzerland) with a 3D Gaussian filter constrained at σ = 1.0 and support = 2 for partial suppression of the noise in the volumes. All the micro-CT data was processed with Mimics 21.0 software at a threshold of 2500 to discriminate new bone tissue from surrounding tissues and polymer/HA scaffold and a cylindrical region of interest (ROI) with a diameter of 5.0 × 3.0 mm was chosen to evaluate the newly regenerated bone. Bone volume/total volume (BV/TV) was calculated. All analyses were repeated with four specimens.

2.10. Histological analysis

Tissues were sectioned and fixed in 4 % phosphate buffered paraformaldehyde solution for histological assessment. The sections were stained with hematoxylin and eosin (H&E) and Masson's trichrome (Hematoxylin Staining Solution, FZ-025, Eosin Staining Solution, FZ-028, Masson's trichrome stain solution, FZ-037, Hebei Bio-High Technology Development CO., LTD, China.) to observe the new bone formation and collagen deposition, respectively, within the wound areas. Digital images from each experimental group were acquired by an optical microscope (40×, 100×, and 400× magnification).

2.11. Statistical analysis

All quantitative data is presented as mean ± SD with a minimum of three independent samples and analyzed by one-way analysis of variance (ANOVA). P values < 0.05 were regarded as statistically significant.

3. Results and discussion

3.1. POC-βGP-Na and POC-GP-Ca are incorporated into citrate-based materials

The synthesis of POC-GP is similar to that for POC through a one pot polycondensation of citric acid, 1,8-octanediol and βGP-Na/-Ca to obtain the POC-βGP-Na/-Ca pre-polymers, which can be further crosslinked (post-polymerization) to prepare polymer films (Fig. 1A). It should be noted that after the pre-polymer synthesis, both POC-βGP-Na/POC-GP-Ca pre-polymers were purified via dialysis before lyophilization to remove soluble and unreacted monomers. Investigated formulations of the POC-βGP-Na and POC-GP-Ca are listed in Table 1.

Next, the chemical structures of POC and POC-βGP-Na were determined by ^{31}P NMR and FT-IR spectroscopy. In ^{31}P NMR spectra (Fig. 1B), the peak at −1.19 ppm was assigned to phosphate triester group (PO_4^{3-}) from βGP-Na while no peak was shown in the spectrum of POC, indicating the successful incorporation of βGP-Na in POC-βGP-Na pre-polymer. In FT-IR (Fig. 1C), the strong peak at 1705 cm^{-1} was assigned to the ester group (—C(=O)OR), the broad peak at 2932 cm^{-1} was from methylene groups in 1,8-octanediol, and the broad band at 3470 cm^{-1} represented hydroxyl groups (—OH). The band at 1194 cm^{-1} as shown in POC indicated the stretch vibration of C—O in ester groups. Due to the electron coupling between phosphate and carboxyl group, the peak of C—O shifted to a lower wavelength number (1170 cm^{-1}) in POC-βGP-Na and POC-GP-Ca [29]. The FT-IR results further confirmed the successful synthesis of POC-βGP-Na and POC-GP-Ca.

3.2. GP incorporation improved mechanical strength

Next, we performed tensile mechanical tests on both POC-βGP-Na and POC-GP-Ca polymer films (Fig. 2 & Table 2). For POC-GP-Na, its mechanical properties were significantly affected by the feeding ratio of βGP-Na, evidenced by the tensile stress-strain curves (Fig. 2A), in which POC-0.2βGP-Na and POC-0.3βGP-Na displayed classical stress-stain curves of elastomers similar to POC, while POC-0.5βGP-Na showed a curve of plastic deformation. More importantly, by increasing the hydrophilic βGP-Na content, the initial tensile modulus was increased about 72 times from POC (3.55 ± 0.35 MPa) to POC-0.5βGP-Na (256.44 ± 22.8 MPa), and the tensile strength was elevated about 11 times from POC (2.5 ± 0.18 MPa) to POC-0.5βG-PNa (28.2 ± 2.44 MPa). More importantly, the introduction of GP-Ca into POC could further
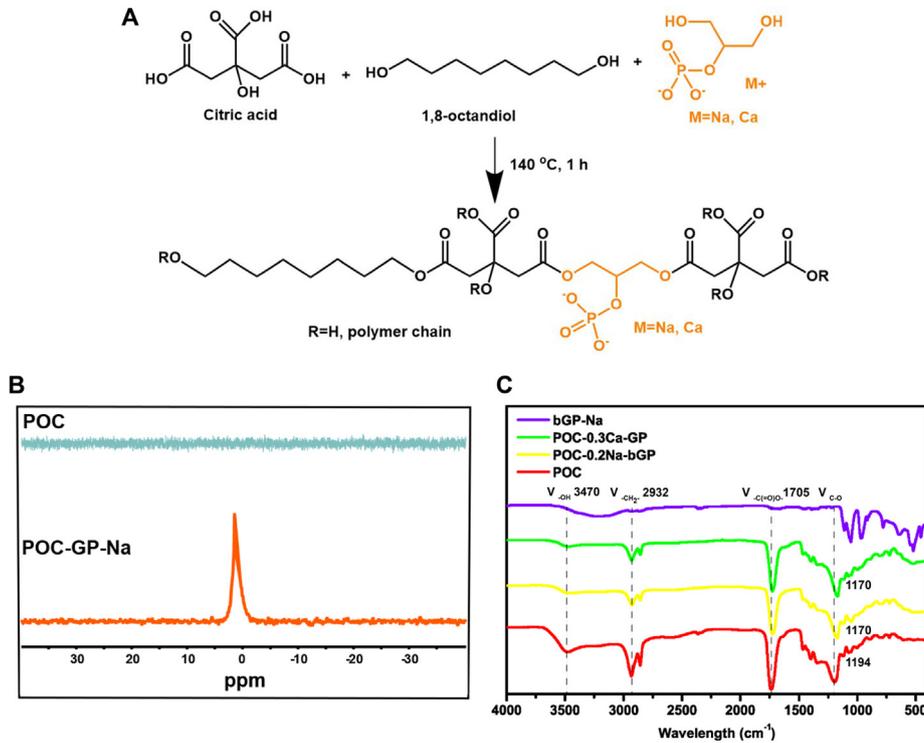
Fig. 1. Synthesis and Characterization of POC-GP polymers. (A) Schematic representation of POC-GP pre-polymer synthesis. (B) ^{31}P-NMR analysis of the POC-GP polymers. (C) FT-IR analysis of POC-GP pre-polymers.
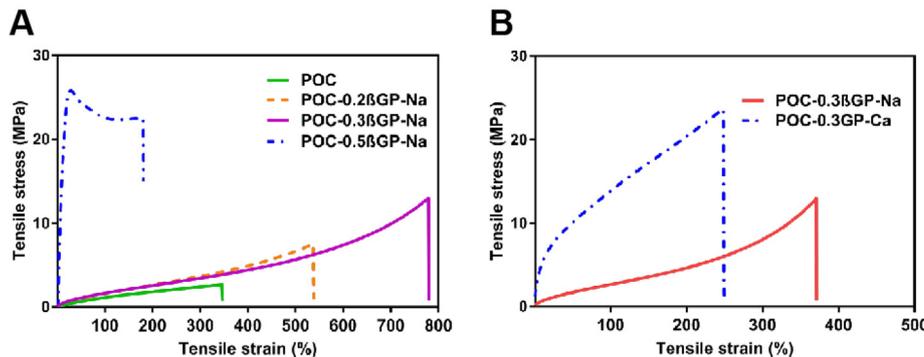
Fig. 2. Mechanical properties of POC-GP films. (A) Stress-strain curves of POC, POC-0.2βGP-Na, POC-0.3βGP-Na, and POC-0.5βGP-Na polymers. (B) Stress-strain curves of POC-0.3GP-Ca in comparison with POC-0.3βGP-Na.

Table 2
Improved mechanical properties of the POC-GP crosslinked polymer films in comparison with POC.

	Young's Modulus (MPa)	Tensile strength (MPa)	Elongation (%)
POC	3.55 ± 0.35	2.50 ± 0.18	144 ± 28
POC-0.2βGP-Na	5.28 ± 0.56	7.45 ± 1.63	270 ± 52
POC-0.3βGP-Na	5.81 ± 0.11	13.36 ± 3.77	361 ± 34
POC-0.5βGP-Na	256.44 ± 22.88	28.20 ± 2.44	15.7 ± 4.2
POC-0.2GP-Ca	10.65 ± 2.65	13.06 ± 0.59	182 ± 26
POC-0.3GP-Ca	55.08 ± 9.68	22.76 ± 1.06	199 ± 7.0

Thermo-crosslinking conditions: 3 days at 80 °C and 1 day at 120 °C under vacuum.

improve the material's mechanical strength. As shown in Fig. 2B, POC-0.3GP-Ca (22.76 ± 1.06 MPa) exhibited significantly higher tensile strength than the POC-0.3βGP-Na (13.36 ± 3.77 MPa). By changing the GP salt type during synthesis, the initial tensile mod-

ulus was increased (Table 2) about 9 times from POC-0.3βGP-Na (5.81 ± 0.11 MPa) to POC-0.3GP-Ca (55.08 ± 9.68 MPa), probably due to the improved polymer crosslinking between ionic calcium and the citrate polymer network. The above results demonstrated the addition of GP salts and choice of GP salts could be adopted as a convenient way to modulate the mechanical properties of the resultant citrate polymers. Also, the tensile strengths of the resultant POC-GP polymer films without HA reinforcement, ranging from 5.28 ± 0.56 MPa to 28.20 ± 2.44 MPa, are similar to that of natural skin (1–20 MPa) and within the range of articular cartilage (9–40 MPa) [30], suggesting that the mechanically tunable POC-GP polymers may potentially meet the mechanical requirements of different tissue applications.

3.3. Degradation rate of POC-GP can be tuned by GP incorporation

The wettability of POC-GP films was evaluated by water-in-air contact angle tests using POC as control. As shown in Fig. 3A, the
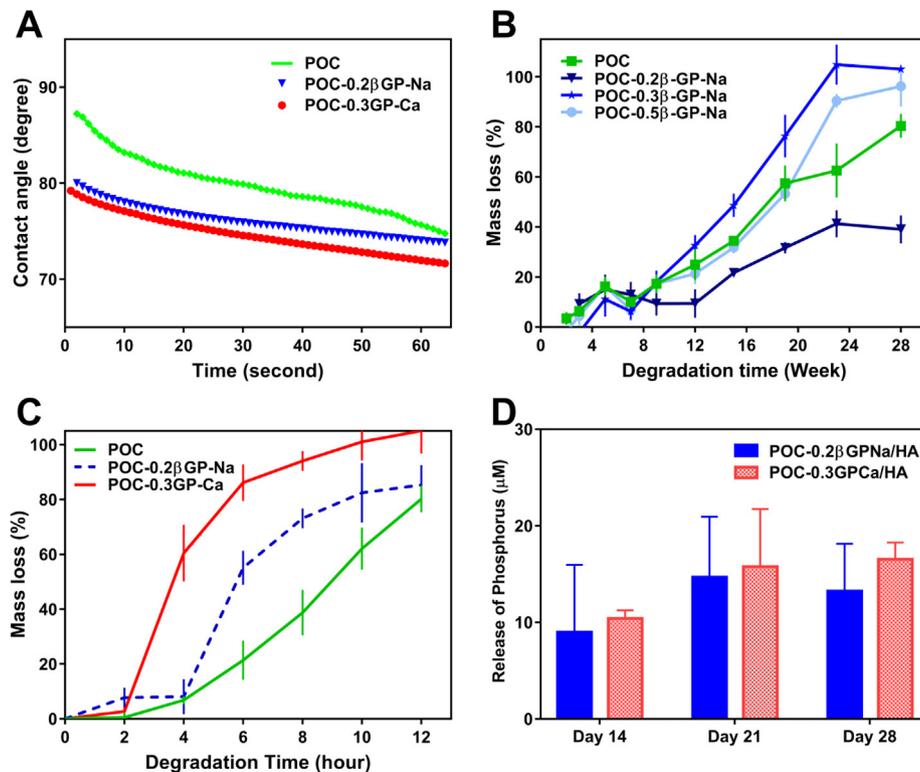
Fig. 3. Contact angle test and degradation of POC-GP films. (A) Contact angle changes over time tested on the POC-0.2βGP-Na and POC-0.3GP-Ca crosslinked polymer films. (B) Degradation of POC and POC-βGP-Na polymer films in PBS (C) Accelerated degradation of POC, POC-0.2βGP-Na and POC-0.3GP-Ca polymer films in 0.05 M NaOH. (D) Cumulative release of phosphorus from POC-0.2βGP-Na and POC-0.3GP-Ca films.

contact angle of both POC-βGP-Na and POC-GP-Ca was lower than that of POC initially, but became close to that of POC after 60 s, indicating the hydrophilic nature of POC-GP backbones with similar wettability to POC. Considering the material's degradation may affect cell responses, tissue penetration and the life-span of the implants [31], we sought to screen the *in vitro* degradation rate of different polymers in an accelerated manner in 0.05 M NaOH. In order to tune the material degradation, the monomer ratios of βGP-Na over citric acid were varied. Interestingly, degradation studies in phosphate buffered saline (PBS) showed that the increase of βGP-Na feeding ratios from 0.2 to 0.3 in POC polymer network accelerated the degradation rates (Fig. 3B), but further increase of the GP-Na feeding ratio (POC-0.5βGP-Na) resulted in slower degradation as compared with that of POC. As suggested in Fig. 3A, adding GP salts into POC slightly improved the wettability, resulting in faster degradation of POC-0.2βGP-Na over POC. However, increasing βGP-Na in POC resulted in the loss of elasticity, especially for POC-0.5βGP-Na that might become semi-crystalline (Fig. 2A), leading to slower degradation. For accelerated degradation as shown in Fig. 3C, POC-βGP-Na and POC-GP-Ca all showed a faster degradation speed than POC in 0.05 M NaOH, suggesting that adding GPs significantly affects the degradation of the resultant polymers. The accelerated degradation data were also in agreement with the contact angle data showing that POC-βGP-Na and POC-GP-Ca have similar wettability but a more hydrophilic character than POC. Overall, the degradation of POC-GP was expected to be variable and can be tuned by hydrophilicity of monomers, monomer feeding ratios, and polymer chain length [1,32]. Further, ICP-OES revealed the accumulative release of phosphorus from both POC-βGP-Na and POC-GP-Ca polymer films during degradation in PBS gradually increased from 9.00 ± 6.93 μM to 13.24 ± 4.89 μM, and 10.41 ± 0.84 μM to 16.53 ± 1.74 μM for POC-βGP-Na and POC-GP-Ca, respectively (Fig. 3D). It was reported that

both GP monomers and inorganic phosphate could play a favorable osteopromotive role in bone healing and formation [18]. Together with our previous findings that citrate, as an osteopromotive factor, could also be released from citrate-based polymers [18], the above results strongly suggested that citrate- and GP-presenting POC-GP materials may be highly beneficial for their use in orthopedic applications.

3.4. POC-GP/HA composites favored hMSCs differentiation in vitro

To evaluate the potential of both POC-GP materials for orthopedic application, the cytocompatibility of the new materials with different ratio of GP salts was first assessed by culturing hMSCs on the crosslinked polymer films for 24 h before the cell viability was tested by CCK-8. Polycaprolactone (PCL) films and Blank wells without polymer films were used as controls. As shown in Fig. 4, it was obvious that POC-GP-Ca films exhibited good cytocompatibility with less than 20 % viability reduction compared with the blank control, which is comparable with that of commercial PCL films, but better than that of POC-βGP-Na. In all three POC-βGP-Na formulations, by increasing the feeding ratios of βGP-Na to citric acid from 0.2 to 0.5, there was a significant decrease in cell viability, indicating that overuse of βGP-Na may cause a toxicity concern. Proliferation of hMSCs on different polymer films was also tested by using CCK8, which showed that all POC-βGP-Na polymer films supported cell proliferation at least to a similar extent of PCL control films. Notably, POC-0.3GP-Ca films elicited a comparable proliferation rate of hMSCs to that in the blank control group, but are better than that on the PCL films. The above results demonstrated the excellent cytocompatibility of POC-βGP-Na and POC-GP-Ca as implantable materials. POC-0.2βGP-Na and POC-0.3GP-Ca were selected and named as POC-βGP-Na and POC-GP-Ca, respectively, for the following stem cell differentiation and *in vivo* studies.
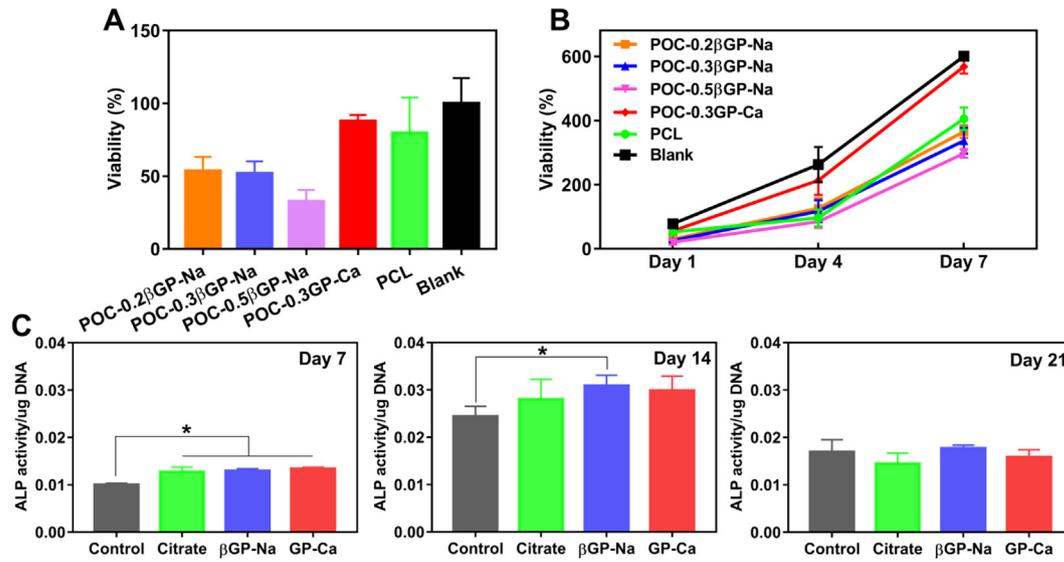
Fig. 4. Cytocompatibility test of POC-GP films. (A) Cytotoxicity evaluation of hMSCs cultured on different polymer films at 24 h. (B) Proliferation of hMSCs on different polymer films for 1,4 and 7 days. (C) Effect of two GP salts, βGP-Na and GP-Ca, and citrate at concentrations of 200 μM on hMSCs osteogenic differentiation, evaluated by ALP expression.

Soluble citrate at 200 μM supplemented in established osteogenic medium has been found to be the optimal concentration to promote osteogenesis progression [18], and β-GP-Na in its solute form (from 2 mM to 10 mM) is already included in the osteogenic medium; however, the effect of GP-Ca, a food supplement for calcium and phosphate, on osteo-differentiation of stem cells has not been well studied, probably due to the low solubility of GP-Ca at pH 7.5 (around 5.7 mg/mL) [34]. Therefore, in order to identify the effect of citrate, GP-Na and GP-Ca on hMSC differentiation, we prepared reductive osteogenic medium including only dexamethasone and ascorbate-2-phosphate and then supplemented with citrate, GP-Na or GP-Ca at 200 μM for hMSC culture. As shown in Fig. 4C, the ALP expression in either βGP-Na, GP-Ca, or citrate group was significantly higher than that in control group on day 7, while

on day 21 no difference in ALP level between all groups was found, suggesting their comparable osteopromotive effect mainly at the early-to-middle stage of differentiation.

To mimic the natural bone composition, POC-βGP-Na and POC-GP-Ca pre-polymers composited with 60 % HA by weight were fabricated into flat disks before crosslinking. POC/60%HA and PLGA/35%HA composite disks were also prepared as controls. To evaluate the potential of POC-GP/HA composites in orthopedic applications, hMSCs were differentiated on different composites in osteogenic medium and the production of alkaline phosphatase (ALP) was tested after 7, 14, and 21 days. A significant increase in ALP expression was observed on POC-GP-Ca/HA at all three time points tested, as compared to all other groups (Fig. 5A). In comparison, the incorporation of POC-βGP-Na did not appear to further
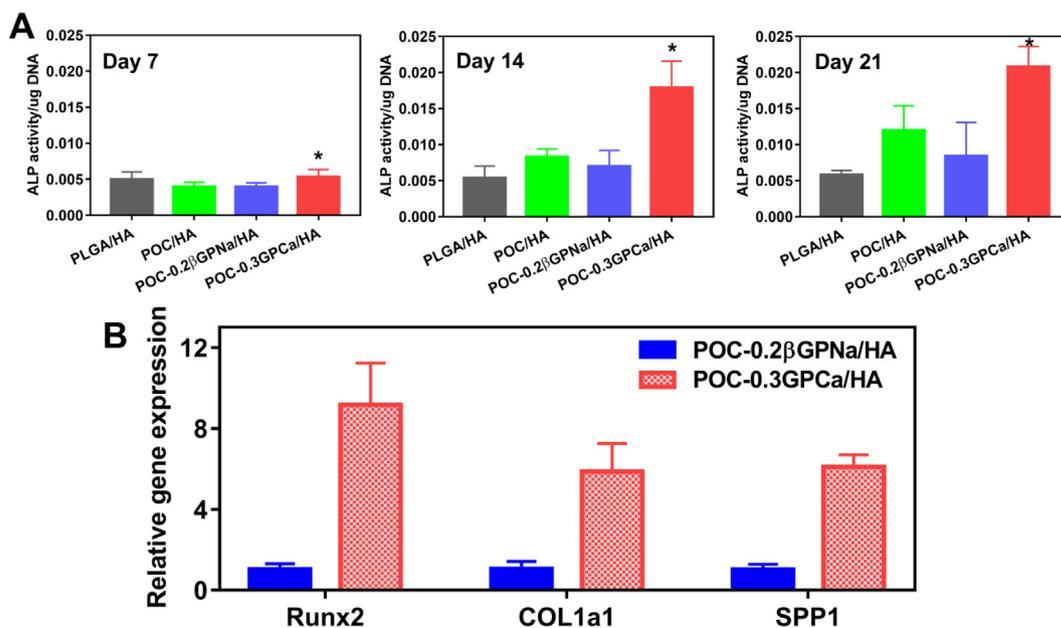
Fig. 5. Osteogenic differentiation on hMSCs on composite materials. (A) ALP production of hMSCs differentiation on the POC/HA, POC-βGP-Na/HA and POC-GP-Ca/HA composite disks in osteogenic medium for 7, 14, and 21 days, compared with that on PLGA/HA (* indicating P < 0.05). (B) Gene expression of *Runx-2*, *Col1a1*, and *SPP1* in differentiating hMSCs cultured on polymer composites for 14 days, as analyzed by real-time PCR (* indicating P < 0.05).

promote osteogenic differentiation, with similar ALP production levels of stem cells cultured on POC-βGP-Na/HA to that on POC/HA. Also, as expected, all citrate-based composites supported enhanced osteogenic differentiation, as compared to the PLGA/HA composites, especially on day 14 and 21, consistent with our pre-

vious studies showing the osteopromotive capability of citrate-based composites [18,33].

Real-time PCR revealed a marked increase in all three osteogenic markers (*Runx-2*, Collagen type I and osteopontin) when culturing hMSCs on POC-GP-Ca/HA compared to POC-βGP-Na/HA in
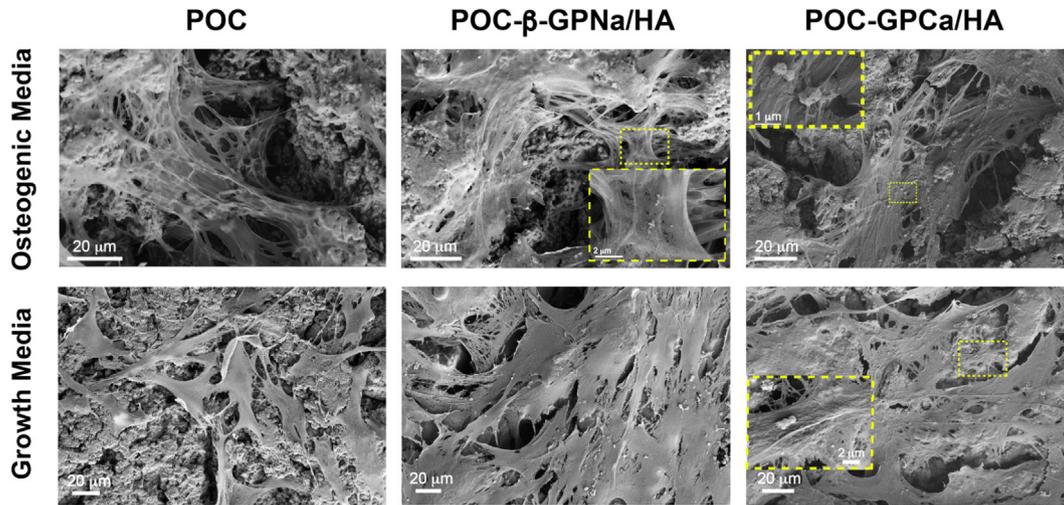
Fig. 6. SEM observation of mineral deposits and ECM formation for hMSCs cultured on composites in osteogenic medium and in growth medium.
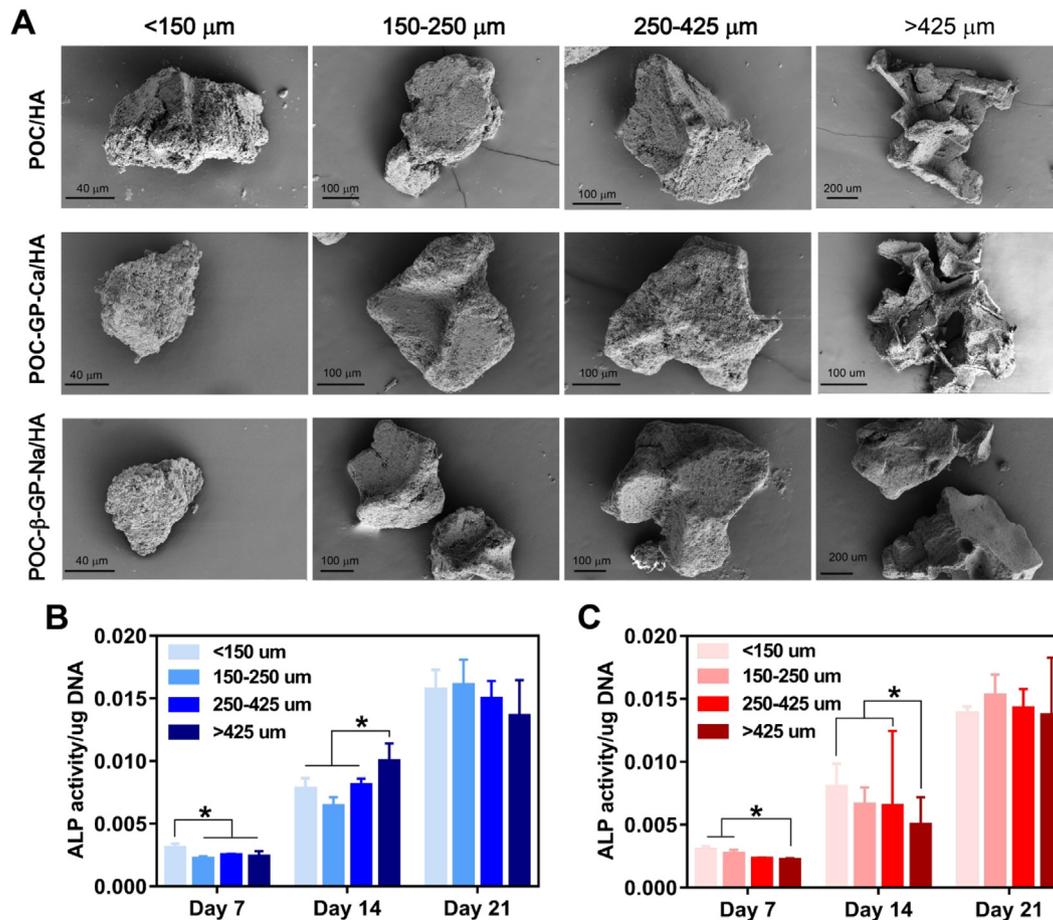
Fig. 7. Composite microparticles and the effect of microparticle size on osteogenic differentiation. (A) SEM images of the composite microparticles at different size ranges (<150 μm; 150–250 μm; 250–425 μm; >425 μm). (B) ALP production of hMSCs differentiation in reductive osteogenic medium on POC-βGP-Na/HA and POC-GP-Ca/HA composite microparticles at different size ranges for 7, 14, and 21 days (* indicating P < 0.05).

established osteogenic medium. The results suggested that the more cytocompatible POC-GP-Ca/HA provided better support for hMSC osteogenic progression and bone related extracellular matrix production (collagen type I and osteopontin), confirming a superior osteopromotive effect of POC-GP-Ca/HA over POC-βGP-Na/HA. Meanwhile, the extracellular matrix and calcium deposits produced by hMSCs at 14 days were observed by SEM. As shown in Fig. 6, when cultured in established osteogenic medium, the formation of fibrous extracellular matrix was evident in all three material groups with more calcium deposits formed in both POC-GP groups. When cultured in growth medium, cells tended to display normal stem cell morphology with smooth cell surface, except in the POC-GP-Ca/HA group where signs of fibrous extracellular matrix were evident. Small amounts of calcium deposits were also observed in both POC-GP/HA groups. Taken together, the above results revealed that although soluble βGP-Na and GP-Ca possess comparable osteopromotive effect, and the prepared POC-βGP-Na/HA and POC-GP-Ca/HA composites both supported the in vitro formation of calcium deposits by releasing βGP-Na and GP-Ca as organic donor, POC-GP-Ca/HA composites, in comparison with POC-βGP-Na/HA, were more supportive for osteogenic progression and the production of bone-related extracellular matrix, probably due to its excellent cytocompatibility and its relatively faster degradation to release osteopromotive citrate and GP-Ca. Considering that organic phosphate availability and the cell produced ECM network (serving as biomineralization template) both are

critical for cell-mediated biomineralization, POC-GP-Ca/HA composites might be a superior candidate for orthopedic applications.

3.5. POC-GP/HA composite microparticles supported hMSCs differentiation in vitro

To further translate POC-GP for orthopedic applications, we fabricated the POC-βGP-Na/HA and POC-GP-Ca/HA composites into microparticulate scaffolds by preparing crosslinked porous polymer/60%HA composite scaffolds through salt leaching (pore size: 250–425 μm), followed by grinding and sieving. Microparticles at different size ranges (<150 μm; 150–250 μm; 250–425 μm; >425 μm) were obtained and POC/HA microparticles were also prepared as control. The surface features of three different kinds of microparticles at different sizes were observed by Scanning Electron Microscope (SEM; Fig. 7A), which showed a more evident "ridge" surface feature on microparticles with larger particles size (>250 μm), and a rougher surface on microparticles with smaller particle size (<150 μm), probably due to the exposure of bioactive HA through grinding. Next, in order to explore the effect of particle size on osteogenic differentiation, we differentiated hMSCs on both POC-βGP-Na/HA and POC-GP-Ca/HA microparticles at different size ranges. The ALP production of hMSCs revealed a similar trend for both POC-βGP-Na/HA and POC-GP-Ca/HA microparticles (Fig. 7B), that is, microparticles with the size of <150 μm promoted the osteo-differentiation at early time point (day 7), probably
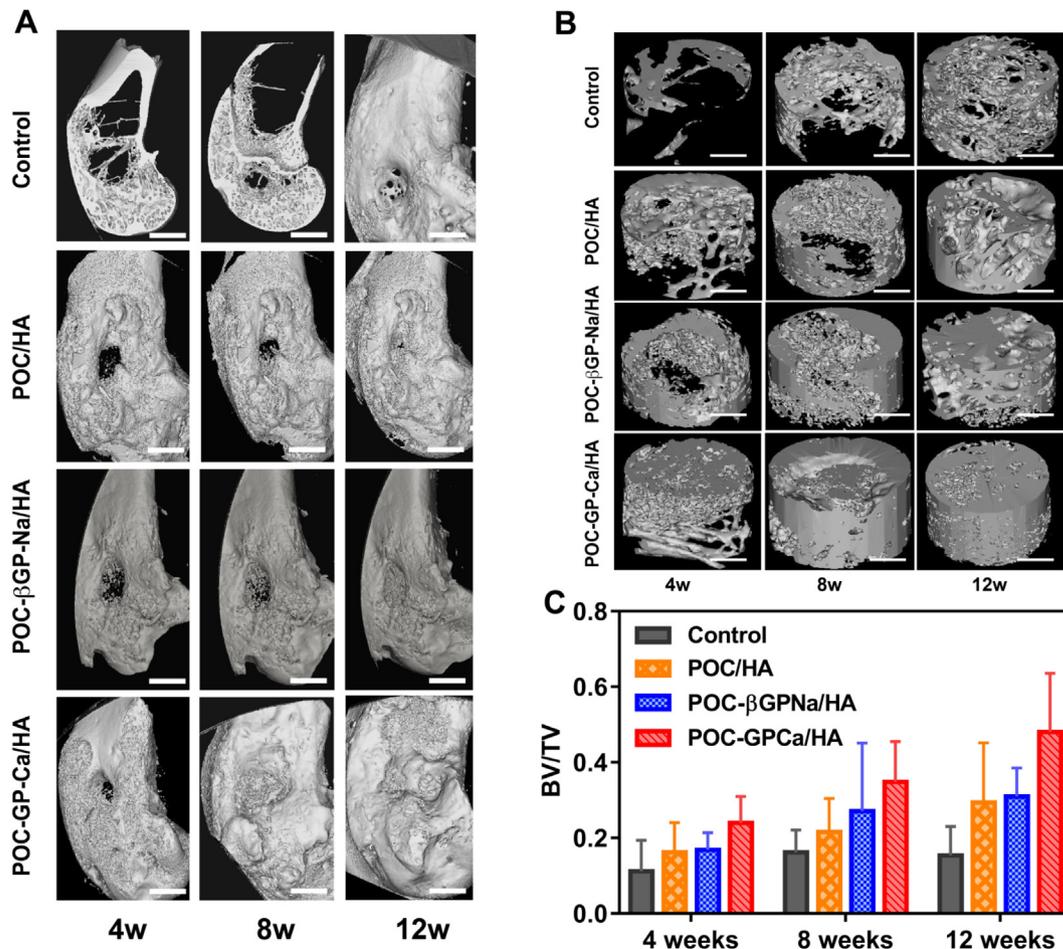
Fig. 8. Micro-CT evaluation of new bone formation. (A) 3D reconstructed micro-CT images of the femoral condyle defects at 1, 2, and 3 months after implantation. Scale bar: 5 mm. (B) 3D reconstructed micro-CT images of the new bone formation within the defects at 1, 2, and 3 months after implantation. Scale bar: 1 mm. (C) Quantitative micro-CT analysis of the BV/TV value to evaluate new bone formation.

because of the more exposed bioactive HA; while larger size of microparticles were shown to favor ALP production when the differentiation proceeded to middle stages (day 14), probably due to the rough surface feature facilitating cell adhesion and 3D interaction for differentiation [18]. Eventually, at late stage (day 21), hMSCs cultured on microparticles with different sizes all produced ALP to a similar extent. Therefore, a mixture of microparticles of different sizes were used in the following *in vivo* evaluation of their capability to support bone regeneration.

3.6. POC-GP/HA microparticles promoted bone regeneration in femoral condyle defects

Based on the results from *in vitro* studies, we further investigated the *in vivo* osteopromotion functionality of both POC-βGP-Na/HA and POC-GP-Ca/HA microparticle scaffolds in a rabbit femoral condyle defect, a standardized and reproducible defect model without the need for fixation that has been successfully applied to evaluate the efficacy of particulate bone grafts in bone repair [18,35]. POC/HA microparticles were also implanted as material control, while defects without any implants served as negative control. At 4, 8 and 12 weeks after implantation, micro-CT analysis was performed to evaluate the new bone formation within defects. The 3D reconstructed images (Fig. 8A) of the defects clearly showed new bone ingrowth in all three scaffold groups occurring from the defect edge towards the defect center, resulting in a gradual decrease of defect size. The bone ingrowth speed in all three scaffold groups was much higher than that in the control group without any microparticles implanted, although new bone ingrowth was also observed in the control group from 4 to 12 weeks. 3D reconstructed images of new bone formation within defects also support the above conclusion (Fig. 8B), displaying significantly less density signal in the Control group than that in the three materials groups at each time point. Moreover, both Fig. 8A and B showed an enhanced new bone formation in the POC-GP-

Ca/HA group, as compared with that in POC-βGP-Na/HA and POC/HA group. Compared with the previously developed CBPB/HA, iCMBA/HA and BPLP-PSer, which were also citrate-based polymer/HA composites, POC-GP-Ca/HA showed excellent osteointegration ability and reached a complete new born ingrowth surrounding implants in a relatively short time (8 weeks) [15,16,18]. Quantitative micro-CT analysis data (Fig. 8C) further confirmed a significantly higher BV/TV value in the POC-GP-Ca/HA group as compared to other control groups, especially at 12 weeks. These *in vivo* results supported the superior performance of POC-GP-Ca/HA microparticles in promoting new bone formation, which is consistent with the *in vitro* differentiation results (Fig. 5).

Histological analysis of the newly formed tissue within the defects were further performed. In the representative Masson staining images of three different microparticles at 1 month of implantation (Fig. 9), blue-stained immature bone growing from the defect edge towards its center through the microparticle scaffolds, with intimate interaction between new bone and materials with fibrous connective tissue in the defect center was observed in all material groups. There is no separation, such as fibrous capsule between the implants and host bone tissue, demonstrating the excellent osteoconductivity and osteointegration of all citrate-based composite microparticles. At 2-month post implantation, more blue-stained bone was found to deposit directly onto the microparticles, while red-stained mature bone started to be visible around the POC-GP-Ca/HA implants, suggesting that the POC-GP-Ca/HA might favor bone maturation compared with other control groups. H&E staining images at 1 month (Fig. 10A & B) further confirmed a close contact between the new bone and both POC-βGP-Na/HA and POC-GP-Ca/HA microparticles. The connective tissue in POC-GP-Ca/HA group (Fig. 10D) that intertwined with microparticles in the defect center and close to the bone growth front seemed to be denser than that in the POC-βGP-Na/HA group even after 2 months (Fig. 10C). Direct bone deposition with osteoblasts
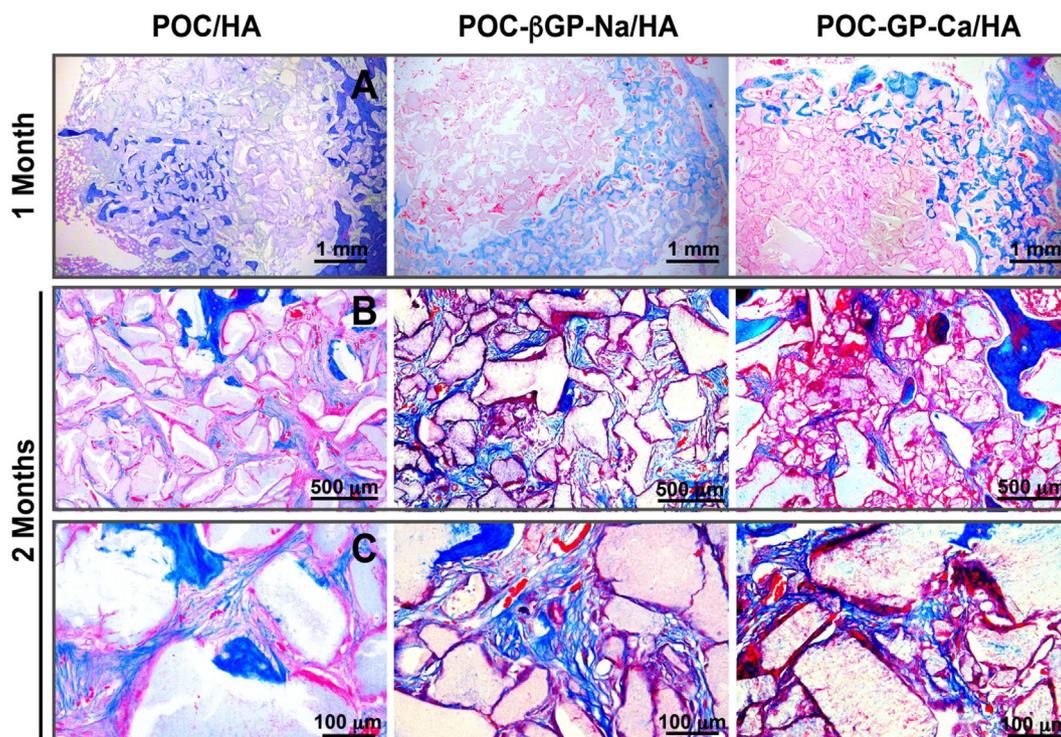
Fig. 9. Masson staining images of the newly formed bone within the defects implanted with POC/HA, POC-βGPNa/HA and POC-GPCa/HA at (A) 1 month, and (B-C) 2 months post-implantation.

POC-βGP-Na/HA
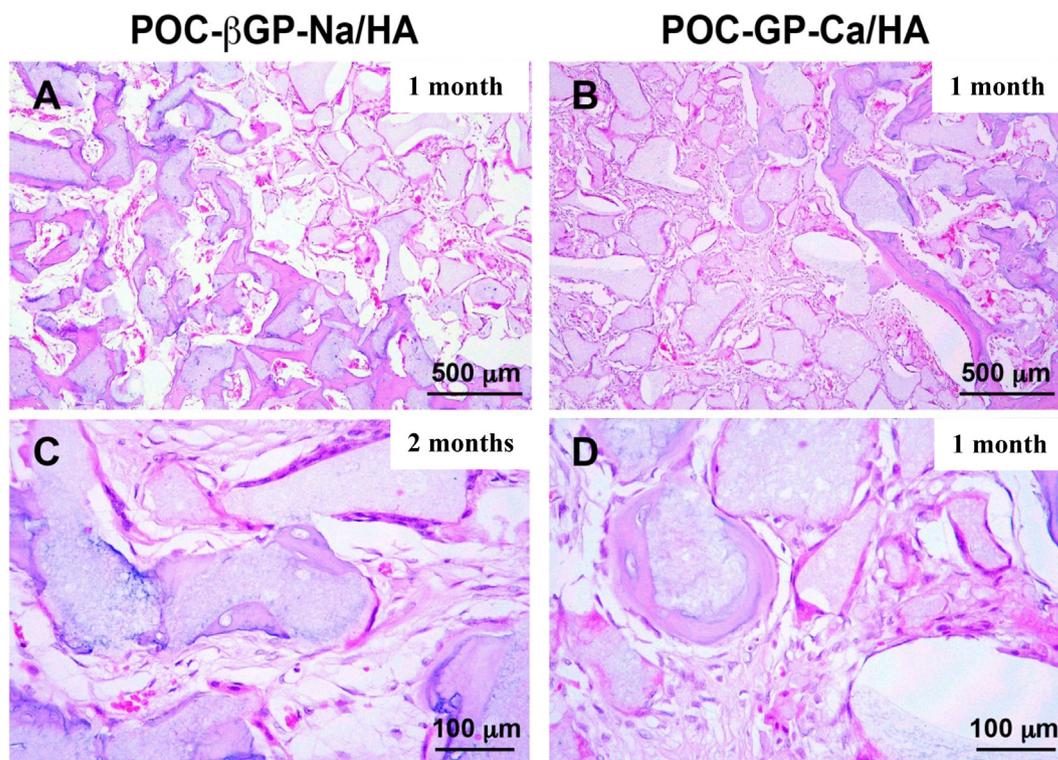
POC-GP-Ca/HA

Fig. 10. H&E staining images of tissues surrounding microparticle implants. (A) POC-βGP-Na/HA at 1 month; and (B) POC-GP-Ca/HA at 1 month (scale bar = 500 μm). (C) POC-βGP-Na/HA at 2 months and (D) POC-GP-Ca/HA at 1 month (scale bar = 100 μm).

lined up around the microparticles and with visible trapped osteocytes were observed in the POC-GP-Ca/HA group at 1 month and in the POC-GP-Na/HA group at 2 months. Together with the micro-CT analysis, these results consistently suggested that POC-GP-Ca/HA microparticles possessed excellent osteoconductivity and promoted bone regeneration in the femoral condyle defects, serving as a better candidate than POC-βGP-Na/HA for orthopedic applications.

4. Conclusions

In conclusion, in the present study we developed a new class of osteopromotive bioactive biodegradable materials, POC-βGP-Na and POC-GP-Ca with widely tunable mechanical properties and degradation. POC-GPs could be synthesized by a simple and cost-effective polycondensation method. Within the formulations investigated, POC-GP-Ca/HA composites demonstrated better bioactivity in promoting osteopromotive differentiation of hMSCs *in vitro* and further improving bone regeneration in rabbit femoral condyle defects. The development of POC-GP expands the repertoire of the well-recognized citrate-based biomaterials to meet the ever-increasing needs for functional biomaterials in tissue engineering and other biomedical applications.

Acknowledgements

Conflict of interest

Dr. Yang and The Pennsylvania State University have a financial interest in Acuitive Technologies, Inc. These interests have been reviewed by the University's Institutional and Individual Conflict of Interest Committees and are currently being managed by the University.

References

[1] C. Laurencin, Y. Khan, S.F. El-Amin, Bone graft substitutes, Expert Rev. Med. Devices 3 (1) (2006) 49–57.

[2] V. Campana, G. Milano, E. Pagano, M. Barba, C. Cicione, G. Salonna, W. Lattanzi, G. Logroscino, Bone substitutes in orthopaedic surgery: from basic science to clinical practice, J. Mater. Sci.: Mater. Med. 25 (10) (2014) 2445–2461.

[3] J. Song, V. Malathong, C.R. Bertozzi, Mineralization of synthetic polymer scaffolds: a bottom-up approach for the development of artificial bone, J. Am. Chem. Soc. 127 (10) (2005) 3366–3378.

[4] S. Bhumiratana, W.L. Grayson, A. Castaneda, D.N. Rockwood, E.S. Gil, D.L. Kaplan, G. Vunjak-Novakovic, Nucleation and growth of mineralized bone matrix on silk-hydroxyapatite composite scaffolds, Biomaterials 32 (11) (2011) 2812–2820.

[5] B.M. Chesnutt, A.M. Viano, Y. Yuan, Y. Yang, T. Guda, M.R. Appleford, J.L. Ong, W.O. Haggard, J.D. Bumgardner, Design and characterization of a novel chitosan/nanocrystalline calcium phosphate composite scaffold for bone regeneration, J. Biomed. Mater. Res. A 88 (2) (2009) 491–502.

[6] S.L. Liang, W.D. Cook, G.A. Thouas, Q.Z. Chen, The mechanical characteristics and in vitro biocompatibility of poly(glycerol sebacate)-bioglass elastomeric composites, Biomaterials 31 (33) (2010) 8516–8529.

[7] H. Liu, T.J. Webster, Mechanical properties of dispersed ceramic nanoparticles in polymer composites for orthopedic applications, Int. J. Nanomed. 5 (2010) 299–313.

[8] R.L. Hartles, Citrate in mineralized tissues, Adv. Oral Biol. 1 (1964) 225–253.

[9] Y.Y. Hu, X.P. Liu, X. Ma, A. Rawal, T. Prozorov, M. Akinc, S.K. Mallapragada, K. Schmidt-Rohr, Biomimetic self-assembling copolymer−hydroxyapatite nanocomposites with the nanocrystal size controlled by citrate, Chem. Mater. 23 (9) (2011) 2481–2490.

[10] C. Ma, E. Gerhard, D. Lu, J. Yang, Citrate chemistry and biology for biomaterials design, Biomaterials 178 (2018) 383–400.

[11] R.T. Tran, J. Yang, G.A. Ameer, Citrate-based biomaterials and their applications in regenerative engineering, Ann. Rev. Mater. Res. 45 (2015) 277–310.

[12] E.J. Chung, P. Kodali, W. Laskin, J.L. Koh, G.A. Ameer, Long-term in vivo response to citric acid-based nanocomposites for orthopaedic tissue engineering, J. Mater. Sci. Mater. Med. 22 (9) (2011) 2131–2138.

[13] Y. Guo, R.T. Tran, D. Xie, Y. Wang, D.Y. Nguyen, E. Gerhard, J. Guo, J. Tang, Z. Zhang, X. Bai, J. Yang, Citrate-based biphasic scaffolds for the repair of large segmental bone defects, J. Biomed. Mater. Res. A 103 (2) (2015) 772–781.

[14] D. Sun, Y. Chen, R.T. Tran, S. Xu, D. Xie, C. Jia, Y. Wang, Y. Guo, Z. Zhang, J. Guo, J. Yang, D. Jin, X. Bai, Citric acid-based hydroxyapatite composite scaffolds enhance calvarial regeneration, Sci. Rep. 4 (2014) 6912--6922.

[15] R.T. Tran, L. Wang, C. Zhang, M. Huang, W. Tang, C. Zhang, Z. Zhang, D. Jin, B. Banik, J.L. Brown, Z. Xie, X. Bai, J. Yang, Synthesis and characterization of biomimetic citrate-based biodegradable composites, J. Biomed. Mater. Res. A 102 (8) (2014) 2521–2532.

[16] D. Xie, J. Guo, M. Mehdizadeh, R.T. Tran, R. Chen, D. Sun, G. Qian, D. Jin, X. Bai, J. Yang, Development of injectable citrate-based bioadhesive bone implants, J. Mater. Chem. B, Mater. Biol. Med. 3 (3) (2015) 387–398.

[17] J. Tang, J. Guo, Z. Li, C. Yang, D. Xie, J. Chen, S. Li, S. Li, G.B. Kim, X. Bai, Z. Zhang, J. Yang, Fast degradable citrate-based bone scaffold promotes spinal fusion, J. Mater. Chem. B, Mater. Biol. Med. 3 (27) (2015) 5569–5576.

[18] C. Ma, X. Tian, J.P. Kim, D. Xie, X. Ao, D. Shan, Q. Lin, M.R. Hudock, X. Bai, J. Yang, Citrate-based materials fuel human stem cells by metabonegenic regulation, Proc. Natl. Acad. Sci. 115 (50) (2018) 11741–11750.

[19] S. Prasadh, R.C.W. Wong, Unraveling the mechanical strength of biomaterials used as a bone scaffold in oral and maxillofacial defects, Oral Sci. Int. 15 (2) (2018) 48–55.

[20] J. Dey, H. Xu, J. Shen, P. Thevenot, S.R. Gondi, K.T. Nguyen, B.S. Sumerlin, L. Tang, J. Yang, Development of biodegradable crosslinked urethane-doped polyester elastomers, Biomaterials 29 (35) (2008) 4637–4649.

[21] J. Guo, Z. Xie, R.T. Tran, D. Xie, D. Jin, X. Bai, J. Yang, Click chemistry plays a dual role in biodegradable polymer design, Adv. Mater. 26 (12) (2014) 1906–1911.

[22] S. Saravanan, S. Vimalraj, P. Thanikaivelan, S. Banudevi, G. Manivasagam, A review on injectable chitosan/beta glycerophosphate hydrogels for bone tissue regeneration, Int. J. Biol. Macromol. 121 (2019) 38–54.

[23] E.-H. Song, K.-I. Cho, H.-E. Kim, S.-H. Jeong, Biomimetic coating of hydroxyapatite on glycerol phosphate-conjugated polyurethane via mineralization, ACS Omega 2 (3) (2017) 981–987.

[24] J. Kucińska-Lipka, I. Gubanska, O. Korchynskyi, K. Malysheva, M. Kostrzewa, D. Włodarczyk, J. Karczewski, H. Janik, The influence of calcium glycerophosphate (GPCa) modifier on physicochemical mechanical, and biological performance of polyurethanes applicable as biomaterials for bone tissue scaffolds fabrication, Polymers 9 (8) (2017) 329–350.

[25] S. Morochnik, Y. Zhu, C. Duan, M. Cai, R.R. Reid, T.C. He, J. Koh, I. Szleifer, G.A. Ameer, A thermoresponsive, citrate-based macromolecule for bone regenerative engineering, J. Biomed. Mater. Res. Part A 106 (6) (2018) 1743–1752.

[26] T. Holland, E. Bodde, V. Cuijpers, L. Baggett, Y. Tabata, A. Mikos, J. Jansen, Degradable hydrogel scaffolds for in vivo delivery of single and dual growth factors in cartilage repair, Osteoarthritis Cartilage 15 (2) (2007) 187–197.

[27] L.A. Solchaga, J.S. Temenoff, J. Gao, A.G. Mikos, A.I. Caplan, V.M. Goldberg, Repair of osteochondral defects with hyaluronan-and polyester-based scaffolds, Osteoarthritis Cartilage 13 (4) (2005) 297–309.

[28] Y. Liu, X.Z. Shu, G.D. Prestwich, Osteochondral defect repair with autologous bone marrow-derived mesenchymal stem cells in an injectable situ, cross-linked synthetic extracellular matrix, Tissue Eng. 12 (12) (2006) 3405–3417.

[29] M.I. Tejedor-Tejedor, M.A. Anderson, Protonation of phosphate on the surface of goethite as studied by CIR-FTIR and electrophoretic mobility, Langmuir 6 (1990) 602–612.

[30] G.A. Holzapfel, Biomechanics of soft tissue, in: The Handbook of Materials Behavior Models 3, 2001, pp. 1049–1063.

[31] H.J. Sung, C. Meredith, C. Johnson, Z.S. Galis, The effect of scaffold degradation rate on three-dimensional cell growth and angiogenesis, Biomaterials 25 (26) (2004) 5735–5742.

[32] J. Hu, K. Peng, J. Guo, D. Shan, G.B. Kim, Q. Li, E. Gerhard, L. Zhu, W. Tu, W. Lv, M. A. Hickner, J. Yang, Click cross-linking-improved waterborne polymers for environment-friendly coatings and adhesives, ACS Appl. Mater. Interfaces 8 (2016) 17499–117410.

[33] H. Qiu, J. Yang, P. Kodali, J. Koh, G.A. Ameer, A citric acid-based hydroxyapatite composite for orthopedic implants, Biomaterials 27 (34) (2006) 5845–5854.

[34] S.L. Goss, K.A. Lemons, J.E. Kerstetter, R.H. Bogner, Determination of calcium salt solubility with changes in pH and PCO2, simulating varying gastrointestinal environments, J. Pharm. Pharmacol. 59 (11) (2007) 1485–1492.

[35] M.J. Coathup, Q. Cai, C. Campion, T. Buckland, G.W. Blunn, The effect of particle size on the osteointegration of injectable silicate-substituted calcium phosphate bone substitute materials, J. Biomed. Mater. Res. B Appl. Biomater. 101 (6) (2013) 902–910.